Widespread tissue distribution and synthetic pathway of polyunsaturated C24:2 sphingolipids in mammals

Mai Edagawa, Megumi Sawai, Yusuke Ohno, Akio Kihara*

Laboratory of Biochemistry, Faculty of Pharmaceutical Sciences, Hokkaido University, Sapporo, Japan

*Corresponding author

Address correspondence to:

Akio Kihara

Laboratory of Biochemistry

Faculty of Pharmaceutical Sciences, Hokkaido University

Kita 12-jo, Nishi 6-chome, Kita-ku, Sapporo 060-0812, Japan

Telephone: +81-11-706-3754

Fax: +81-11-706-4900

E-mail: kihara@pharm.hokudai.ac.jp

Abstract

Sphingolipids are multifunctional lipids and a major constituent of the cell membranes of eukaryotes. Although the fatty acid (FA) moiety of sphingolipids is usually a saturated or monounsaturated FA, polyunsaturated FA (PUFA)-containing species also exist in mammalian tissues. In the present study, we showed that C24:2 PUFA-containing ceramide is one of the seven major ceramide species in a wide range of tissues. C24:2 ceramide levels were especially high in spleen and small intestine; in the former, it was the fourth most abundant ceramide species. However, both the synthetic pathway and the physiological function of C24:2 ceramide had yet to be identified. Tracer analysis using deuterium-labeled linoleic acid (C18:2) revealed that C24:2 ceramide is produced via elongation of linoleic acid. We also found that the FA elongase ELOVL1 and the ceramide synthase CERS2 were involved in C24:2 ceramide production. Sphingolipids are known to form lipid microdomains in membranes; however, in a detergent-resistant membrane (DRM) assay, we observed a lower proportion of C24:2 sphingomyelin in the DRM fraction than of saturated sphingomyelins, suggesting that C24:2 sphingolipids may act to negatively regulate lipid microdomain formation. Our findings expand our knowledge of sphingolipid diversity, and provide insight into how different sphingolipid molecular species play different functions in biological membranes.

Keywords: ceramide, fatty acid, lipid, lipid microdomain, polyunsaturated fatty acid, sphingolipid

Abbreviations: BSA, bovine serum albumin; DRM, detergent-resistant membrane; FA, fatty

acid; HexCer, monohexosylceramide; KO, knockout; LC, liquid chromatography; LCB, long-chain base; LCFA, long-chain fatty acid; MS, mass spectrometry; MS/MS, tandem mass spectrometry; PC, phosphatidylcholine; PI, phosphatidylinositol; PUFA, polyunsaturated fatty acid; VLC, very long-chain; VLCFA, very long-chain fatty acid.

1. Introduction

Sphingolipids, together with glycerophospholipids and cholesterol, constitute the biological membranes of eukaryotes. Sphingolipids play several important physiological roles including in neural function, skin barrier formation, regulation of glucose metabolism, recognition of bacterial toxins and viruses, spermatogenesis, immunity, and vascular formation and function [1-5]. They are enriched in the outer leaflet of plasma membranes, where they cluster to form so-called lipid microdomains [6, 7]. These structures serve as platforms where many cell signaling proteins accumulate to promote efficient signal transduction.

Complex sphingolipids—i.e., sphingomyelin and glycosphingolipids in mammals—consist of the hydrophobic backbone ceramide and a polar head group (phosphocholine in sphingomyelin and a saccharide chain in glycosphingolipids). Mammals possess hundreds of glycosphingolipid species that differ in their sugar residues and linking modes [5]. The simplest among these are glucosylceramide and galactosylceramide, having only one glucose and galactose residue respectively; they are collectively referred to as monohexosylceramides (HexCers) or cerebrosides.

Ceramide is composed of a long-chain base (LCB) and a fatty acid (FA). LCBs commonly contain hydroxyl groups at C1 and C3 and an amino group at C2 [5, 8]. These functional groups act as donors and acceptors of hydrogen bonds to form lipid microdomains. In contrast, glycerophospholipids have only acceptors for hydrogen bonds but no hydrogen bond donors. The major mammalian LCB is sphingosine (d18:1; where d indicates 2 (double) hydroxyl groups; 18, carbon chain length; 1, number of double bonds) with a *trans* double bond between C4 and C5. Mammals also have other LCBs including sphingadienine

(d18:2)—which contains a *trans* double bond between C4 and C5 and a *cis* double bond between C14 and C15—and saturated dihydrosphingosine (d18:0) [8, 9].

According to chain length, cellular FAs can be classified into long-chain FAs (LCFAs) with C11–C20 and very long-chain (VLC) FAs (VLCFAs) with ≥C21 [10, 11]. FA compositions differ between glycerophospholipids and sphingolipids. Most glycerophospholipids contain LCFAs as their FA moiety [12], while many sphingolipids contain VLCFAs, especially C24:0 and C24:1 FAs. About 30–70% of sphingomyelins containing VLCFAs, with specific proportions varying among tissues [11]. In addition, glycerophospholipids often contain polyunsaturated FAs (PUFAs) such as linoleic acid (C18:2) and arachidonic acid (C20:4), mostly at the *sn*-2 position [12]. Since the *cis* double bonds of PUFAs are bent in membranes, glycerophospholipids do not readily cluster with each other. In contrast, the FA moiety of sphingolipids is mainly saturated C16-C24, although monounsaturated sphingolipids with C24:1 also exist ubiquitously [11]. PUFA-containing sphingolipids have only been reported in limited tissues/cells at low levels [13-17]. An exception is spermatozoa (and possibly the surrounding testis), which possesses relatively high amounts of PUFA-containing sphingolipids with ≥C28 [18]. Sphingolipids are typically characterized by hydrophobic chains that do not have *cis* double bonds, allowing the lipids to pack tightly and create hydrophobic interactions, which are further enhanced by long FA chain length. The presence of hydrogen bond donors/acceptors and saturated VLCFAs in sphingolipids drive the formation of lipid microdomains.

Mammals absorb LCFAs from their diet; palmitic acid (C16:0) specifically can also be produced by FA synthase. Fractions of these LCFAs are elongated to VLCFAs via the FA elongation cycle in the endoplasmic reticulum [10, 11]. In each cycle, the FA substrate in

acyl-CoA form is elongated by 2 carbons. The rate-limiting step of the cycle is catalyzed by FA elongases, of which mammals have seven varieties (ELOVL1–7) with different substrate specificities (Fig. 1) [5, 10, 11]. Mammals can produce the monounsaturated FAs palmitoleic acid (C16:1) and oleic acid (C18:1) from palmitic acid and stearic acid (C18:0), respectively, by Δ9 desaturase. However, since mammals lack both Δ12 and Δ15 desaturases, they cannot produce the n-6 PUFA linoleic acid (C18:2) or the n-3 PUFA α-linolenic acid (C18:3), which must therefore be absorbed from dietary sources. Fractions of these PUFAs are elongated by ELOVLs and desaturated by Δ5 and/or Δ6 desaturases to become other n-6 and n-3 PUFAs (Fig. 1). Ceramide synthases produce a ceramide using an acyl-CoA molecule and a LCB as substrates. Mammals have six ceramide synthases (CERS1–6) with different substrate specificities (Fig. 1) [5, 19-21]. Of these, CERS2 is known to be involved in the production of C22 and C24 ceramides [13, 19, 21, 22].

Recent developments in mass spectrometry (MS) now allow lipid molecules to be analyzed in detail. In particular, triple quadrupole-type mass spectrometers can distinguish among lipids having the same molecular mass but different structures by tandem mass spectrometry (MS/MS) [23]. For example, d18:1-C24:1 ceramide and d18:2-C24:0 ceramide have the same molecular mass but can be distinguished by the differences in their daughter ions. Combining liquid chromatography (LC) with triple quadrupole MS makes it possible to separate and identify even more lipid species. In the present study, we used LC-MS/MS to perform detailed analyses on ceramide species from various mouse tissues. Although PUFA-containing sphingolipids had only been reported in limited tissues [14-18], we found here that C24:2 sphingolipids exist relatively abundantly in a wide range of tissues. Furthermore, we revealed the synthetic pathway of C24:2 ceramide.

2. Material and methods

2.1. Cell culture

HAP1, near-haploid human cells derived from myelogenous leukemia [24], and HeLa cells were grown in Iscove's modified Dulbecco's medium (Thermo Fisher Scientific, Waltham, MA, USA) and Dulbecco's modified Eagle's medium (Sigma, St. Louis, MO, USA), respectively, with each medium supplemented with 10% fetal bovine serum, 100 units/ml penicillin, and 100 μg/ml streptomycin.

2.2. Mice

C57BL/6J mice were purchased from Sankyo Labo Service Corporation (Tokyo, Japan). *Elovl1*$^{-/-}$ *Tg*(*IVL-Elovl1*) mice have been described previously [25]. Mice were housed in a 23 ± 1 °C environment in a 12-h light/dark cycle and were fed standard chow diet (PicoLab Rodent Diet 20; LabDiet, St. Louis, MO, USA), and water *ad libitum*. The animal experiments were approved by the institutional animal care and use committees of Hokkaido University.

2.3. LC–MS/MS analysis

Lipids were extracted from spleen and small intestine tissue (~50 mg) collected from *Elovl1*$^{-/-}$ *Tg*(*IVL-Elovl1*) mice and wild type control mice (C57BL/6J) at 1 month old, or else HeLa and HAP1 cells (~10^6 cells), by vigorous mixing (4,500 rpm) with 450 μl of chloroform/methanol/12 M formic acid (100:200:1, v/v) in tubes containing zirconia beads for 1 min using a Micro Smash MS-100 (TOMY Seiko, Tokyo, Japan). Samples were mixed in a low temperature room (4 °C), during which time the sample temperature increased to

about 25 °C. After centrifugation (20,000 × g, 3 min, 4 °C), the supernatant was recovered, mixed with 150 µl of chloroform and 270 µl of water, and subjected to phase separation by centrifugation (20,000 × g, 3 min, 4 °C). The organic phase was recovered, dried, dissolved in 5,000 µl (for tissues) or 150 µl (for cells) of chloroform/methanol (1:2, v/v), and analyzed by LC-MS/MS as described below.

Although the above method had high quantitative performance for cell samples, it was only semi-quantitative for tissues, due to the low lipid extraction efficiency and large sample mass (50 mg). Therefore, in our ceramide quantification experiments, we reduced the tissue mass to 10 mg and performed lipid extraction twice. Brain, lung, heart, skeletal muscle, spleen, kidney, liver, colon, small intestine, and testis tissue from C57BL/6J mice at 1 month old and epidermis at postnatal day 0 were prepared and treated with 30 pmol of internal standard (LIPIDMAPS™ Mass Spec Internal Standard, Ceramide/Sphingoid Internal Standard Mix I; Avanti Polar Lipids, Alabaster, AL, USA). Lipids were extracted with 450 µl of chloroform/methanol/12 M formic acid (100:200:1, v/v) as described above using the Micro Smash MS-100. After centrifugation (20,000 × g, 3 min, room temperature), the supernatant was recovered. The pellet was dissolved in 450 µl of chloroform/methanol/1 M formic acid (100:200:1, v/v), and lipids were extracted again. After centrifugation (20,000 × g, 3 min, room temperature), the supernatant was recovered. Next, the two supernatants were pooled, mixed with 300 µl of chloroform and 540 µl of water, and subjected to phase separation by centrifugation (20,000 × g, 3 min, room temperature). The organic phase was recovered, dried, dissolved in 1,500 µl of chloroform/methanol (1:2, v/v), and analyzed by LC-MS/MS as described below. Due to its naturally high levels of ceramide, epidermis was diluted 50-fold with chloroform/methanol (1:2, v/v) before LC-MS/MS.

LC-MS/MS analyses were performed by ultra-performance LC on a reverse-phase column (ACQUITY UPLC CSH C18 column, 2.1 × 100 mm, particle size 1.7 μm; Waters, Milford, MA, USA) coupled with electrospray ionization tandem triple quadrupole MS (Xevo TQ-S; Waters) essentially as described previously [26-28]. LC was conducted at 55 °C (column temperature) with a flow rate of 0.3 ml/min in a binary gradient system with mobile phase A (acetonitrile/water (3:2, v/v) containing 5 mM ammonium formate) and mobile phase B (acetonitrile/2-pronanol (9:1, v/v) containing 5 mM ammonium formate). Elution gradient steps were as follows: 0 min, 10% B; 0–6 min, gradient to 40% B; 6–15 min, gradient to 70% B; 15–18 min, gradient to 100% B; 18–23 min, 100% B; 23–23.1 min, gradient to 10% B; 23.1–25 min, 10% B. Ceramide, sphingomyelin, and HexCer species were detected in positive ion mode, whereas phosphatidylcholine (PC) and phosphatidylinositol (PI) species were detected in negative ion mode via multiple reaction monitoring, by selecting specific *m/z* (mass to charge ratio) values for the quadrupole mass filters Q1 and Q3 (Tables S1-S5) with specific collision energies (ceramides, 32 eV; sphingomyelins, 60 eV, HexCers, 40 eV; PCs, 50 eV; and PIs, 55 eV). MassLynx software (Waters) was used for data analysis and quantification.

2.4. Lipid labeling assay

HeLa cells were incubated with 5 μM d_{11}-linoleic acid (Cayman Chemical, Ann Arbor, MI, USA), having 11 deuterium atoms per molecule, at 37 °C for 48 h. Lipids were extracted and dried as described previously [28]. For measuring sphingomyelins, dried lipids were dissolved in 225 μl chloroform/methanol (1:1, v/v) and subjected to alkaline treatment to hydrolyze PC, the presence of which can confound sphingomyelin measurement, as follows.

Samples were incubated with 71 µl of 0.5 M NaOH for 1 h at 37 °C, then neutralized with 35.5 µl of 1 M formic acid. Lipids were extracted by successive additions of 106.5 µl of chloroform and 219 µl of water with mixing. Phases were separated by centrifugation, and the organic phase was recovered, dried, dissolved in chloroform/methanol (1:2, v/v), and analyzed by LC-MS/MS as described above.

2.5. Construction of CERS2 knockout (KO) HAP1 cells

CERS2 KO cells were produced by a CRISPR/Cas9 nickase system using HAP1 cells. The all-in-one CRISPR/Cas9 vector pYU417 consists of a *Cas9 D10A* mutant nuclease (*Cas9* nickase), a guide RNA cloning cassette, *EGFP*, and the puromycin *N*-acetyltransferase gene [28]. For production of two guide RNAs (guide RNA 1 and guide RNA 2; Fig. S1) targeted to *CERS2*, two oligonucleotide pairs (5'-AGAAGTAATCATACAAGGTCGTTTT-3'/5'-GACCTTGTATGATTACTTCTCGGTG-3' and 5'-GCTGCCTGTGAACTTGACCTGTTTT-3'/5'-AGGTCAAGTTCACAGGCAGCCGGTG-3') were each annealed and cloned into pYU417, producing the pMED3 and pMED4 plasmids. HAP1 cells were transfected with the pMED3 and pMED4 plasmids using Lipofectamine Plus Reagent (Thermo Fisher Scientific), according to the manufacturer's instruction. Twenty-four hours after transfection, cells were treated with 2 µg/ml puromycin for two days and then cultured in Iscove's modified Dulbecco's medium without puromycin for additional 7 days. The *CERS2* genomic region of the obtained clones was subjected to DNA sequencing. Three of the obtained clones—characterized respectively by *CERS2* deletions of 40 bp (*CERS2* KO clone 1), 247 bp (clone 2), and 41 bp (clone 3)—were used

for further analyses (Fig. S1).

2.6. Real-time quantitative RT-PCR

Total RNAs were isolated from HAP1 cells using the NucleoSpin RNA II Kit (Takara Bio, Shiga, Japan), followed by conversion to cDNAs using the PrimeScript II 1st strand cDNA Synthesis Kit (Takara Bio), both according to the manufacturer's manuals. Obtained cDNAs were then subjected to real-time quantitative PCR using KOD SYBR qPCR Mix (Toyobo, Osaka, Japan) and primers (*CERS1*, 5'-CTGGCGCAAGGACTCGGTGG-3' and 5'-ATTGTGGTACCGGAAGGCG-3'; *CERS2*, 5'-GCTGGAGTCAGCCAAGATGT-3' and 5'-AGGATCCAGAAGGGCAGGAT-3'; *CERS3*, 5'-GTTTAGGAGTCGGCGGAATCAAG-3' and 5'-AAACGCAATTCCAGCAACAGTG-3'; *CERS4*, 5'-GCAGTATCAGCAAGTGTGCG-3' and 5'-GTGGGAAAGAGGACCAGTCG-3'; *CERS5*, 5'-ATCTTCTTCGTGAGGCTG-3' and 5'-ATGTCCCAGAACCAAGGT-3'; and *CERS6*, 5'-ATCAGGAGAAGCCAAGCACG-3' and 5'-AGTAGTGAAGGTCAGTTGTG-3') on a CFX96 Touch Real-Time PCR Detection System (Bio-Rad, Hercules, CA, USA).

2.7. Preparation of detergent-resistant membrane (DRM) fraction

HeLa cells cultured in a 150 mm dish were washed with PBS, suspended in 870 µl of cold buffer A (50 mM HEPES-NaOH (pH 7.4), 150 mM NaCl, 1 mM dithiothreitol, 1 mM phenylmethylsulfonyl fluoride, 1 × Complete protease inhibitor mixture (EDTA-free; Roche Diagnostics, Indianapolis, IN, USA), 1 mM dithiothreitol, and 1% Triton X-100), and lysed using a homogenizer. After addition and mixing of 870 µl of sucrose solution (85% sucrose, HEPES-NaOH (pH 7.4), and 150 mM NaCl), samples were transferred to an

ultracentrifugation tube. Then, 5.22 ml of 30% sucrose in buffer A, 3.03 ml of 5% sucrose in buffer A, and 2 ml of buffer A were overlaid onto the sample in this order and centrifuged at 250,000 × g at 4 °C for 17 h using a SW41 Ti rotor (Beckman Coulter, Fullerton, CA, USA). Samples were collected from the top: the first 2 ml was designated as fraction 0, and subsequent 1 ml samples as fractions 1–10. Fractions 1–10 were divided into two samples (900 µl for LC-MS/MS analysis and 100 µl for immunoblotting). In the LC-MS/MS analysis, lipids were extracted by successive adding and mixing of 3,375 µl of chloroform/methanol/1 M formic acid (100:200:1, v/v), 1,125 µl of chloroform, and 1,125 µl of water. After centrifugation, the organic phase was recovered, dried, dissolved in chloroform/methanol (1:2, v/v), and analyzed by LC-MS/MS as described above. For immunoblotting, proteins were concentrated by the chloroform-methanol method as described previously [29].

2.8. Immunoblotting

Proteins separated by sodium dodecyl sulfate-polyacrylamide gel electrophoresis were electrotransferred to a Immobilon polyvinylidene difluoride membrane (Millipore, Billerica, MA, USA) at constant current (2 mA/cm^2 membrane) for 1 h using transfer buffer (25 mM Tris, 192 mM glycine, and 20% methanol). The membrane was blocked with 5% bovine serum albumin (Sigma) in TBS-T (20 mM Tris-HCl (pH 7.5), 137 mM NaCl, and 0.05% Tween 20) at 4 °C for 16 h. The membrane was incubated with Can Get Signal Solution 1 (Toyobo) containing the anti-caveolin-1 antibody (D46G3; Cell Signaling Technology, Beverly, MA, USA) at room temperature for 1 h, washed three times with TBS-T, and incubated with Can Get Signal Solution 2 (Toyobo) containing horseradish peroxidase-conjugated anti-rabbit IgG F(ab')$_2$ fragment (1:7500 dilution; GE Healthcare Life

Sciences, Little Chalfont, Buckinghamshire, UK) at 4 °C for 16 h. After washing of the membrane with TBS-T three times, a chemiluminescence reaction was carried out using Western Lightning Plus-ECL (PerkinElmer Life Sciences, Waltham, MA, USA). The signal was detected using an Amersham Imager 600 (GE Healthcare Life Sciences).

3. Results

3.1. C24:2 ceramide exists in a wide range of mouse tissues

Eleven mouse tissues (brain, lung, heart, skeletal muscle, spleen, kidney, liver, colon, small intestine, epidermis, and testis) were checked for levels of sphingosine (d18:1)-containing ceramide species using LC-MS/MS. In this analysis, the *m/z* value 264.3, which corresponds to a part of the sphingosine molecule [23], was used for daughter ion selection with the aim of only measuring sphingosine-containing ceramides (i.e., not measuring ceramides containing other LCBs). In all tissues examined except for epidermis and testis, seven ceramide species (C16:0, C18:0, C20:0, C22:0, C24:0, C24:1, and C24:2 ceramides) were predominant: their sum accounted for >95% of total ceramide content (Fig. 2A; for other ceramide species, see Table S6). Of these species, knowledge about C24:2 ceramide is the most limited: there are only a few reports of its existence [13-17]. However, C24:2 ceramide was detected in a wide range of tissues, existing most abundantly in spleen, followed in descending order by small intestine, colon, lung, and liver (Fig. 2A). In spleen, C24:2 ceramide was the fourth most abundant ceramide species following C24:1, C24:0, and C22:0, and accounted for 10.8% of total ceramide content. Some polyunsaturated ceramides other than C24:2 ceramide was also observed, albeit at much lower levels (Table S6).

Ceramides containing ≥C26 FAs were almost absent in most tissues, but notable levels were detected in epidermis and testis (Fig. 2B and C and Table S6), consistent with previous reports [5, 18, 30]. Fig. 2B and 2C list the top 15 and top 12 ceramide species in epidermis and testis, respectively. Most epidermal ceramides contained saturated and monounsaturated FAs, whereas testis ceramides contained PUFAs, with C30:5 being most abundant. The total amount of ceramide was highest in the epidermis, at levels 28–80 times higher than in the

other tissues (Fig. 2D). Ceramide's abundance in the epidermis can be attributed to its high prevalence in lipid lamellae, multilayered lipid structures that form permeable barriers in the stratum corneum, the outermost epidermis layer [5, 31]. In descending order, the most common ceramide species in epidermis were C26:0, C24:0, C28:0, C26:1, and C22:0. Moreover, substantial amounts of C18:1, C26:1, C28:1, C32:1, and C34:1 unsaturated ceramides existed specifically in epidermis (Fig. 2B). These results indicate that the only polyunsaturated ceramide species with ubiquitous presence in tissues is C24:2.

3.2. C24:2 FA is derived from linoleic acid

The synthetic pathway of C24:2 ceramide has yet to be clarified. We speculated that C24:2 FA is produced from linoleic acid (C18:2) by three rounds of FA elongation, which is then catalyzed to the corresponding ceramide, composed of the C24:2 FA and sphingosine. To test this hypothesis, tracer analysis was performed using deuterium (d_{11})-labeled linoleic acid. Incubation of HeLa cells with 5 μM d_{11}-linoleic acid for 48 h resulted in production of d_{11}-C24:2 ceramide at levels equivalent to non-labeled C24:2 ceramide (Fig. 3A). Few d_{11}-labeled C18:2, C20:2, or C22:2 ceramides were detected. Next, levels of HexCer species in the HeLa cells were measured using the sphingosine-specific *m/z* value 264.3. Again, d_{11}-C24:2 HexCer was detected at levels similar to those of non-labeled C24:2 species (Fig. 3B).

In MS/MS of sphingomyelin, the daughter ion derived from phosphocholine (*m/z* value 184.1) was dominant, while the peak corresponding to the daughter ion derived from sphingosine was too small to be used [23]. Therefore, our analysis could not identify the specific LCB components of sphingomyelins. For example, d18:1-C24:2 sphingomyelin and

d18:2-C24:1 sphingomyelin, which have identical molecular masses, could not be distinguished. The most abundant sphingomyelin species detected was C42:2 (d18:1-C24:1 + d18:2-C24:0) sphingomyelin, followed by C34:1 (d18:1-C16:0 + d18:0-C16:1), C40:1 (d18:1-C22:0 + d18:0-C22:1), C42:1 (d18:1-C24:0 + d18:0-C24:1), C42:3 (d18:1-C24:2 + d18:2-C24:1), and C36:2 (d18:1-C22:1 + d18:2-C22:0) sphingomyelins (Fig. 3C). C42:3 sphingomyelins, including the d18:1-C24:2 species, constituted about 7% of the total sphingomyelin content. Incubation of HeLa cells with 5 μM d_{11}-linoleic acid produced d_{11}-C24:2 sphingomyelin, at levels similar to non-labeled C42:3 (d18:1-C24:2 + d18:2-C24:1) sphingomyelin. In contrast to non-labeled d18:1-C24:2 and d18:2-C24:1 sphingomyelins, which could not be distinguished by LC-MS/MS, our measurements of d_{11}-C24:2 sphingomyelin represent only the d_{11}-C24:2-d18:1 species. Considering that d_{11}-C24:2 sphingomyelin was produced at equivalent levels to the corresponding non-labeled species (as with ceramide and HexCer), it is highly likely that most C42:3 sphingomyelin captured by our measurements is actually d18:1-C24:2 sphingomyelin. We therefore refer to C42:3 sphingomyelin measurements below as C24:2 sphingomyelin, for simplicity. In conclusion, the C24:2 FA portion of C24:2 ceramide is derived from linoleic acid, and C24:2 ceramide is converted to both C24:2 HexCer and C24:2 sphingomyelin.

To investigate whether C24:2 FA is specific to sphingolipids or is also a constituent of glycerophospholipids, we examined molecular species of the glycerophospholipids PC and PI in HeLa cells by LC-MS/MS. The major FA components of PC were C16:0, C16:1, and C18:1 FAs, whereas those of PI were C16:0, C16:1, C18:0, C18:1, and C20:4 FAs (Fig. 3D and E). Almost no PC or PI contained C24:2 FA. Saturated or monounsaturated VLCFAs (C22:0, C22:1, C24:0, and C24:1), which exist in sphingolipids, were also not detected in PC

or PI. Thus, our results suggest C24:2 FA exists specifically in sphingolipids.

3.3. The FA elongase ELOVL1 is involved in C24:2 FA production

C24:2 FA is produced from linoleic acid via three rounds of FA elongation cycles in a CoA form. In our previous *in vitro* analysis, among the seven FA elongases (ELOVL1-7) present in mammals, ELOVL3 exhibited high activity toward C18:2-CoA, while ELOVL5, ELOVL6, and ELOVL7 showed weak activity [32]. This suggests that ELOVL3 is mainly involved in the first of the three FA elongation cycles. The ELOVLs involved in the second (elongation from C20:2 to C22:2) and third cycle (elongation from C22:2 to C24:2) have not yet been determined. ELOVL1 is involved in the elongation of saturated and monounsaturated C20 and C22 FAs [25, 30, 32]. To investigate the involvement of ELOVL1 in C24:2 FA production, we utilized recently produced *Elovl1* mutant mice (*Elovl1*$^{-/-}$ *Tg*(*IVL-Elovl1*)), in which *Elovl1* is disrupted in the whole body except for the epidermis [25]. These mice were produced to circumvent the neonatal lethality observed in conventional *Elovl1* KO mice due to skin barrier defects [30]. Lipids were extracted from the spleen and small intestine, the two tissues with the highest amount of C24:2 ceramide in wild type mice (Fig. 2A), and ceramide species were measured by LC-MS/MS. In spleen, C24:0, C24:1, and C24:2 ceramides were decreased in *Elovl1*$^{-/-}$ *Tg*(*IVL-Elovl1*) mice compared to wild type mice, whereas ≤C22 ceramides were increased (Fig. 4A and Table S7). In small intestine of *Elovl1*$^{-/-}$ *Tg*(*IVL-Elovl1*) mice, C24:0, C24:1, C24:2, and C22:0 ceramides were decreased, while C22:1 and ≤C20 ceramides were increased (Fig. 4B and Table S7). Thus, C24:2 ceramide was decreased by *Elovl1* disruption in both tissues, indicating that ELOVL1 is involved in C24:2 FA production.

3.4. The ceramide synthase CERS2 is involved in C24:2 ceramide synthesis

Mammals have six ceramide synthases (CERS1–6), each showing characteristic substrate specificity (Fig. 1) [5]. Of these, CERS2 catalyzes saturated and monounsaturated C22 and C24 ceramide production [13, 19, 21, 22]. To investigate the involvement of CERS2 in C24:2 ceramide production, *CERS2* KO cells were produced with a CRISPR/Cas9 system using near-haploid human cell line HAP1 [24]. We obtained three *CERS2* KO clones with a 40 bp, 247 bp, and 41 bp deletion, respectively, in and around the exon 2 of *CERS2* (Fig. S1). Expression levels of *CERS* genes in wild type and *CERS2* KO HAP1 cells were examined by quantitative real-time RT-PCR. All *CERS* genes were expressed in HAP1 wild type cells, with *CERS2* having the highest expression (Fig. 5A). Expression levels of the *CERS1*, *CERS3*, *CERS4*, *CERS5*, or *CERS6* were almost unaffected by the *CERS2* deletions. In addition, *CERS2* expression was comparable in wild type and *CERS2* KO cells, indicating that the deletions affected neither the synthesis nor stability of the *CERS2* mRNA. Examination of the ceramide composition in wild type HAP1 cells by LC-MS/MS revealed that C24:0 and C24:1 ceramides were abundant (Fig. 5B), reflecting the high expression levels of *CERS2*. In *CERS2* KO HAP1 cells, levels of C24:2 ceramide, in addition to C22:1, C24:0, and C24:1 ceramides, were reduced compared to wild type cells. In contrast, increases in C18:0 and C20:0 ceramide levels were observed in the *CERS2* KO cells. These results indicate that CERS2 is involved in C24:2 ceramide synthesis.

3.5. C24:2 sphingomyelin localizes outside lipid microdomains

Sphingomyelin is known to form lipid microdomains with cholesterol [7, 33]. The bent

structure of the *cis* double bond in the FA portions of lipids increases intermolecular distances and weakens lipid–lipid interactions. Most glycerophospholipids contain unsaturated FAs with *cis* double bonds. In contrast, many sphingolipids have one *trans* double bond in the LCB moiety (sphingosine), while the FA moiety is saturated. This structural characteristic allows for tight packing of sphingolipids and encourages lipid microdomain formation. Since C24:2 sphingomyelin has two *cis* double bonds, we speculated that it is less able to form lipid microdomains than other sphingomyelin species. To clarify this, we performed a DRM assay, a simple assay for lipid microdomain localization. The non-ionic detergent Triton X-100 was added to HeLa cells, then DRMs were prepared by sucrose density gradient centrifugation. Fraction 3, containing the lipid microdomain marker caveolin-1, was subjected to LC-MS/MS analysis of sphingomyelin species (Fig. 6A). Although saturated sphingomyelins tended to be enriched in the lipid microdomain fraction, the proportion of monounsaturated sphingomyelins was lower than that in the total lipid sample. C24:2 sphingomyelin was even less present in the lipid microdomain fraction; although it accounted for ~7% of total sphingomyelin, it only made up ~2% of the fraction. These results suggest that unsaturated sphingomyelin, especially C24:2 sphingomyelin with two *cis* double bonds, tends to localize outside lipid microdomains.

4. Discussion

In the present study, we examined in detail the ceramide species of mouse tissues and human cells (HeLa and HAP1 cells) by LC-MS/MS analysis, and found that C24:2 ceramide was one of the top seven ceramide species (together with C16:0, C18:0, C20:0, C22:0, C24:0, and C24:1) in a wide range of tissues and cells (Figs. 2, 3, and 5 and Table S6). C24:2 ceramide was particularly abundant in spleen, at the third highest levels among ceramide species. C24:2 ceramide was the only common species among polyunsaturated ceramides.

To date, conversion to γ-linolenic acid (C18:3) by Δ6 desaturase is the only known FA metabolic pathway of linoleic acid (C18:2). However, in the present study, we revealed another FA metabolic pathway of linoleic acid: elongation to C24:2 FA. Our previous *in vitro* analysis revealed that ELOVL3 exhibits high activity toward C18:2-CoA, whereas ELOVL5, ELOVL6, and ELOVL7 show weak activity [32]. In that experiment, ELOVL1, ELOVL2, or ELOVL4 had no activity at all toward C18:2-CoA. Therefore, it is highly likely that conversion from C18:2-CoA to C20:2-CoA is mainly catalyzed by ELOVL3. On the other hand, in the present study we found that the amount of C24:2 ceramide in spleen and small intestine of *Elovl1*$^{-/-}$ *Tg* (*IVL-Elovl1*) mice was much lower than in corresponding wild type tissues (Fig. 4), indicating that ELOVL1 is involved in the conversion of C20:2-CoA to C22:2-CoA and/or C22:2-CoA to C24:2-CoA (Fig. 7). To date, ELOVL1 has only been known to act on saturated and monounsaturated VLC acyl-CoAs. Our results therefore indicate the novel discovery of C22:2-CoA and/or C24:2-CoA as the only polyunsaturated substrate(s) of ELOVL1. In the *CERS2* KO HAP1 cells, C24:2 ceramide levels were lower than in the control HAP1 cells (Fig. 5B), indicating that the C24:2-CoA produced by ELOVL1 is then converted to C24:2 ceramide by CERS2 (Fig. 7).

Although both glycerophospholipids and sphingolipids contain FAs, these lipid classes vary greatly in their specific FA moieties. Glycerophospholipids mainly contain saturated, monounsaturated, and polyunsaturated LCFAs [12] (Fig. 3D and E). Sphingolipids also have LCFAs, but most of them are saturated [11] (Fig. 2A and Table S6). In addition, C22:0, C24:0, and C24:1 FAs as well as C24:2 FA are specific to sphingolipids (Figs. 2 and 3). Differences in the FA species of glycerophospholipids and sphingolipids may correspond to functional differences in biological membranes.

Sphingolipids contain both hydrogen bond acceptors and donors in the ceramide backbone, in contrast to glycerophospholipids, which have only hydrogen bond acceptors in the diacylglycerol backbone. Furthermore, a large fraction of sphingolipids are composed of sphingosine and saturated VLCFAs and thus do not have *cis* double bonds. In contrast, most glycerophospholipids contain unsaturated FAs with *cis* double bonds. Such structural properties of sphingolipids encourage the formation of lipid microdomains. The *cis* double bonds broaden the distance between lipids, and thus weaken hydrogen bonds and hydrophobic interactions. We attribute the reason why more saturated sphingomyelins than monounsaturated sphingomyelins were observed in the lipid microdomain fraction to this property (Fig. 6B). In addition, C24:2 sphingomyelin comprised a smaller proportion of the lipid microdomain fraction than of total membrane lipids in our DRM assay. This result suggests that unsaturated sphingolipids negatively regulate lipid microdomain formation. However, it has been noted that DRM assays may not necessarily reflect the precise composition of lipid microdomains in living cells [7]. Further *in vitro* studies are needed to clarify the differences in the physical properties of C24:2 sphingolipids and saturated/monounsaturated sphingolipids as well as the role of C24:2 sphingolipids in lipid

microdomain formation.

Acknowledgements

We thank Dr. T. Sassa (Hokkaido University) and Dr. K. Abe (Hokkaido University) for the use of *Elovl1*$^{-/-}$ *Tg* (*IVL-Elovl1*) mice and for sharing ideas on C24:2 ceramide, respectively. This work was supported by the Advanced Research and Development Programs for Medical Innovation (AMED-CREST) Grant Number JP18gm0910002 (to A.K.) of the Japan Agency for Medical Research and Development (AMED) and KAKENHI Grant Numbers JP18H03976 and JP18H04664 (to A.K.) from the Japan Society for the Promotion of Science (JSPS).

References

[1] T. Wennekes, R.J. van den Berg, R.G. Boot, G.A. van der Marel, H.S. Overkleeft, J.M. Aerts, Glycosphingolipids–nature, function, and pharmacological modulation, Angew. Chem. Int. Ed. Engl. 48 (2009) 8848-8869.

[2] A.A. Kulkarni, A.A. Weiss, S.S. Iyer, Glycan-based high-affinity ligands for toxins and pathogen receptors, Med. Res. Rev. 30 (2010) 327-393.

[3] M. Rabionet, A. Bayerle, R. Jennemann, H. Heid, J. Fuchser, C. Marsching, S. Porubsky, C. Bolenz, F. Guillou, H.J. Grone, K. Gorgas, R. Sandhoff, Male meiotic cytokinesis requires ceramide synthase 3-dependent sphingolipids with unique membrane anchors, Hum. Mol. Genet. 24 (2015) 4792-4808.

[4] S. Schmitt, L.C. Castelvetri, M. Simons, Metabolism and functions of lipids in myelin, Biochim. Biophys. Acta 1851 (2015) 999-1005.

[5] A. Kihara, Synthesis and degradation pathways, functions, and pathology of ceramides and epidermal acylceramides, Prog. Lipid Res. 63 (2016) 50-69.

[6] G. van Meer, D.R. Voelker, G.W. Feigenson, Membrane lipids: where they are and how they behave, Nat. Rev. Mol. Cell Biol. 9 (2008) 112-124.

[7] E. Sezgin, I. Levental, S. Mayor, C. Eggeling, The mystery of membrane organization: composition, regulation and roles of lipid rafts, Nat. Rev. Mol. Cell Biol. 18 (2017) 361-374.

[8] S.T. Pruett, A. Bushnev, K. Hagedorn, M. Adiga, C.A. Haynes, M.C. Sullards, D.C. Liotta, A.H. Merrill, Jr., Biodiversity of sphingoid bases ("sphingosines") and related amino alcohols, J. Lipid Res. 49 (2008) 1621-1639.

[9] O. Renkonen, E.L. Hirvisalo, Structure of plasma sphingadienine, J. Lipid Res. 10 (1969)

687-693.

[10] A. Kihara, Very long-chain fatty acids: elongation, physiology and related disorders, J. Biochem. 152 (2012) 387-395.

[11] T. Sassa, A. Kihara, Metabolism of very long-chain fatty acids: genes and pathophysiology, Biomol. Ther. 22 (2014) 83-92.

[12] A. Yamashita, T. Sugiura, K. Waku, Acyltransferases and transacylases involved in fatty acid remodeling of phospholipids and metabolism of bioactive lipids in mammalian cells, J. Biochem. 122 (1997) 1-16.

[13] S. Imgrund, D. Hartmann, H. Farwanah, M. Eckhardt, R. Sandhoff, J. Degen, V. Gieselmann, K. Sandhoff, K. Willecke, Adult ceramide synthase 2 (CERS2)-deficient mice exhibit myelin sheath defects, cerebellar degeneration, and hepatocarcinomas, J. Biol. Chem. 284 (2009) 33549-33560.

[14] O. Quehenberger, A.M. Armando, A.H. Brown, S.B. Milne, D.S. Myers, A.H. Merrill, S. Bandyopadhyay, K.N. Jones, S. Kelly, R.L. Shaner, C.M. Sullards, E. Wang, R.C. Murphy, R.M. Barkley, T.J. Leiker, C.R. Raetz, Z. Guan, G.M. Laird, D.A. Six, D.W. Russell, J.G. McDonald, S. Subramaniam, E. Fahy, E.A. Dennis, Lipidomics reveals a remarkable diversity of lipids in human plasma, J. Lipid Res. 51 (2010) 3299-3305.

[15] T. Nabetani, A. Makino, F. Hullin-Matsuda, T.A. Hirakawa, S. Takeoka, N. Okino, M. Ito, T. Kobayashi, Y. Hirabayashi, Multiplex analysis of sphingolipids using amine-reactive tags (iTRAQ), J. Lipid Res. 52 (2011) 1294-1302.

[16] K. Kobayashi, E. Nagata, K. Sasaki, M. Harada-Shiba, S. Kojo, H. Kikuzaki, Increase in secretory sphingomyelinase activity and specific ceramides in the aorta of apolipoprotein E knockout mice during aging, Biol. Pharm. Bull. 36 (2013) 1192-1196.

[17] T. Baba, J.L. Campbell, J.C. Le Blanc, P.R. Baker, In-depth sphingomyelin characterization using electron impact excitation of ions from organics and mass spectrometry, J. Lipid Res. 57 (2016) 858-867.

[18] R. Sandhoff, Very long chain sphingolipids: tissue expression, function and synthesis, FEBS Lett. 584 (2010) 1907-1913.

[19] Y. Mizutani, A. Kihara, Y. Igarashi, Mammalian Lass6 and its related family members regulate synthesis of specific ceramides, Biochem. J. 390 (2005) 263-271.

[20] Y. Mizutani, A. Kihara, Y. Igarashi, LASS3 (longevity assurance homologue 3) is a mainly testis-specific (dihydro)ceramide synthase with relatively broad substrate specificity, Biochem. J. 398 (2006) 531-538.

[21] T. Sassa, T. Hirayama, A. Kihara, Enzyme activities of the ceramide synthases CERS2–6 are regulated by phosphorylation in the C-terminal region, J. Biol. Chem. 291 (2016) 7477-7487.

[22] Y. Pewzner-Jung, O. Brenner, S. Braun, E.L. Laviad, S. Ben-Dor, E. Feldmesser, S. Horn-Saban, D. Amann-Zalcenstein, C. Raanan, T. Berkutzki, R. Erez-Roman, O. Ben-David, M. Levy, D. Holzman, H. Park, A. Nyska, A.H. Merrill, Jr., A.H. Futerman, A critical role for ceramide synthase 2 in liver homeostasis: II. insights into molecular changes leading to hepatopathy, J. Biol. Chem. 285 (2010) 10911-10923.

[23] A.H. Merrill, Jr., M.C. Sullards, J.C. Allegood, S. Kelly, E. Wang, Sphingolipidomics: high-throughput, structure-specific, and quantitative analysis of sphingolipids by liquid chromatography tandem mass spectrometry, Methods 36 (2005) 207-224.

[24] J.E. Carette, M. Raaben, A.C. Wong, A.S. Herbert, G. Obernosterer, N. Mulherkar, A.I. Kuehne, P.J. Kranzusch, A.M. Griffin, G. Ruthel, P. Dal Cin, J.M. Dye, S.P. Whelan, K.

Chandran, T.R. Brummelkamp, Ebola virus entry requires the cholesterol transporter Niemann-Pick C1, Nature 477 (2011) 340-343.

[25] T. Sassa, M. Tadaki, H. Kiyonari, A. Kihara, Very long-chain tear film lipids produced by fatty acid elongase ELOVL1 prevent dry eye disease in mice, FASEB J. 32 (2018) 2966-2978.

[26] Y. Ohno, S. Nakamichi, A. Ohkuni, N. Kamiyama, A. Naoe, H. Tsujimura, U. Yokose, K. Sugiura, J. Ishikawa, M. Akiyama, A. Kihara, Essential role of the cytochrome P450 CYP4F22 in the production of acylceramide, the key lipid for skin permeability barrier formation, Proc. Natl. Acad. Sci. U. S. A. 112 (2015) 7707-7712.

[27] T. Kitamura, N. Seki, A. Kihara, Phytosphingosine degradation pathway includes fatty acid α-oxidation reactions in the endoplasmic reticulum, Proc. Natl. Acad. Sci. U. S. A. 114 (2017) E2616-E2623.

[28] M. Sawai, Y. Uchida, Y. Ohno, M. Miyamoto, C. Nishioka, S. Itohara, T. Sassa, A. Kihara, The 3-hydroxyacyl-CoA dehydratases HACD1 and HACD2 exhibit functional redundancy and are active in a wide range of fatty acid elongation pathways, J. Biol. Chem. 292 (2017) 15538-15551.

[29] D. Wessel, U.I. Flügge, A method for the quantitative recovery of protein in dilute solution in the presence of detergents and lipids, Anal. Biochem. 138 (1984) 141-143.

[30] T. Sassa, Y. Ohno, S. Suzuki, T. Nomura, C. Nishioka, T. Kashiwagi, T. Hirayama, M. Akiyama, R. Taguchi, H. Shimizu, S. Itohara, A. Kihara, Impaired epidermal permeability barrier in mice lacking *Elovl1*, the gene responsible for very-long-chain fatty acid production, Mol. Cell. Biol. 33 (2013) 2787-2796.

[31] B. Breiden, K. Sandhoff, The role of sphingolipid metabolism in cutaneous permeability

barrier formation, Biochim. Biophys. Acta 1841 (2014) 441-452.

[32] Y. Ohno, S. Suto, M. Yamanaka, Y. Mizutani, S. Mitsutake, Y. Igarashi, T. Sassa, A. Kihara, ELOVL1 production of C24 acyl-CoAs is linked to C24 sphingolipid synthesis, Proc. Natl. Acad. Sci. U. S. A. 107 (2010) 18439-18444.

[33] T. Harayama, H. Riezman, Understanding the diversity of membrane lipid composition, Nat. Rev. Mol. Cell Biol. 19 (2018) 281-296.

Figure captions

Fig. 1. FA and ceramide synthetic pathways. FA and ceramide synthetic pathways and involved FA elongases and ceramide synthases in mammals are shown. Cer, ceramide; C, CERS; E, ELOVL, SFA, saturated FA; MUFA, monounsaturated FA; Δ5, Δ5 desaturase; Δ6, Δ6 desaturase; Δ9, Δ9 desaturase.

Fig. 2. Ubiquitous presence of C24:2 ceramide in tissues. (A-D) Lipids were extracted from brain, lung, heart, skeletal muscle (s. muscle), spleen, kidney, liver, small intestine (s. intestine), colon, and testis of 1 month old wild type mice, or epidermis of postnatal day 0 mice, and ceramide species were examined by LC-MS/MS. Amounts of seven predominant ceramide species in brain, lung, heart, skeletal muscle, spleen, kidney, liver, small intestine, and colon (A), the 15 top species in epidermis (B), the 12 top species in testis (C), and total ceramides (D) are shown. Values represent the means ± S.D. from three independent experiments.

Fig. 3. Synthesis of C24:2 ceramide from linoleic acid. (A-C) HeLa cells were labeled with 5 μM d_{11}-linoleic acid (d_{11}) or vehicle (methanol) at 37 °C for 48 h. Lipids were extracted, and ceramides (A), HexCers (B), and sphingomyelins (C) were examined by LC-MS/MS. Values represent the mean ± S.D. from three independent experiments. (C and D) Lipids were extracted from HeLa cells, and PCs (D) and PIs (E) were examined by LC-MS/MS. Values represent the means ± S.D. from three independent experiments.

Fig. 4. Involvement of the FA elongase ELOVL1 in C24:2 ceramide synthesis. (A and B)

Lipids were extracted from spleen (A) and small intestine (B) of wild type (WT) and *Elovl1*$^{-/-}$ *Tg* (*IVL-Elovl1*) (KO) mice, and ceramide species were examined by LC-MS/MS. Values represent the means ± S.D. from three independent experiments. Statistically significant differences are indicated (*p < 0.05, **p < 0.01; *t*-test).

Fig. 5. Involvement of the ceramide synthase CERS2 in C24:2 ceramide production. (A) Total RNAs were prepared from three wild type (WT) control and three *CERS2* KO HAP1 cells and subjected to SYBR green-based real-time quantitative RT-PCR using primers for *CERS1*, *CERS2*, *CERS3*, *CERS4*, *CERS5*, and *CERS6*. Absolute values of the mRNA levels were calculated by comparison with the levels of the PCR products amplified from the corresponding plasmid encoding the respective gene. Values represent the mean ± S.D. from three clones. (B) Lipids were extracted from three wild type control and three *CERS2* KO HAP1 cells, and ceramide species were examined by LC-MS/MS. Values represent the means ± S.D. from three clones. Statistically significant differences are indicated (*p < 0.05, **p < 0.01; *t*-test).

Fig. 6. Existence of C24:2 sphingomyelins outside lipid microdomains. (A and B) DRM fractions were prepared from HeLa cells by stepwise sucrose gradient centrifugation, and proteins (A) and lipids (B) were prepared from each fraction. (A) Proteins were separated by sodium dodecyl sulfate-polyacrylamide gel electrophoresis, followed by immunoblotting with anti-caveolin-1 antibody. (B) Sphingomyelin species were examined by LC-MS/MS. Values represent the means ± S.D. from three independent reactions. Statistically significant differences are indicated (*p < 0.05, **p < 0.01; *t*-test).

Fig. 7. Proposed C24:2 ceramide synthetic pathway. C18:2-CoA (linoleoyl-CoA) is first elongated to C20:2-CoA by the FA elongase ELOVL3. ELOVL1 is involved in the subsequent C20:2-CoA to C22:2-CoA and/or C22:2-CoA to C24:2-CoA conversion. The ceramide synthase CERS2 catalyzes amide bond formation between C24:2-CoA and a LCB, producing C24:2 ceramide. The dashed box indicates the new metabolic pathway of linoleic acid revealed in the present study. E, ELOVL; Δ5, Δ5 desaturase; Δ6, Δ6 desaturase.

Figure 1

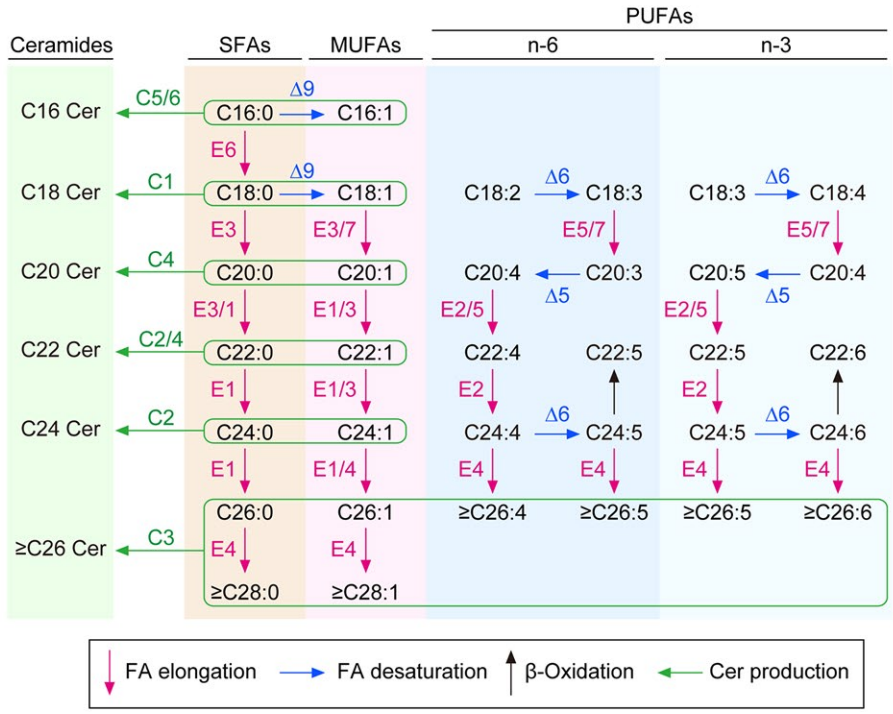
PUFAs
Ceramides
SFAs
MUFAs
n-6
n-3
C16 Cer
C18 Cer
C20 Cer
C22 Cer
C24 Cer
≥C26 Cer
C5/6
C1
C4
C2/4
C2
C3
Δ9
Δ6
Δ5
C16:0
C16:1
C18:0
C18:1
C18:2
C18:3
C18:4
C20:0
C20:1
C20:4
C20:3
C20:5
C20:4
C22:0
C22:1
C22:4
C22:5
C22:5
C22:6
C24:0
C24:1
C24:4
C24:5
C24:5
C24:6
C26:0
C26:1
≥C26:4
≥C26:5
≥C26:5
≥C26:6
≥C28:0
≥C28:1
E6
E3
E3/7
E5/7
E3/1
E1/3
E2/5
E1
E1/3
E2
E1
E1/4
E4
E4
E4
E4
FA elongation
FA desaturation
β-Oxidation
Cer production

Figure 2

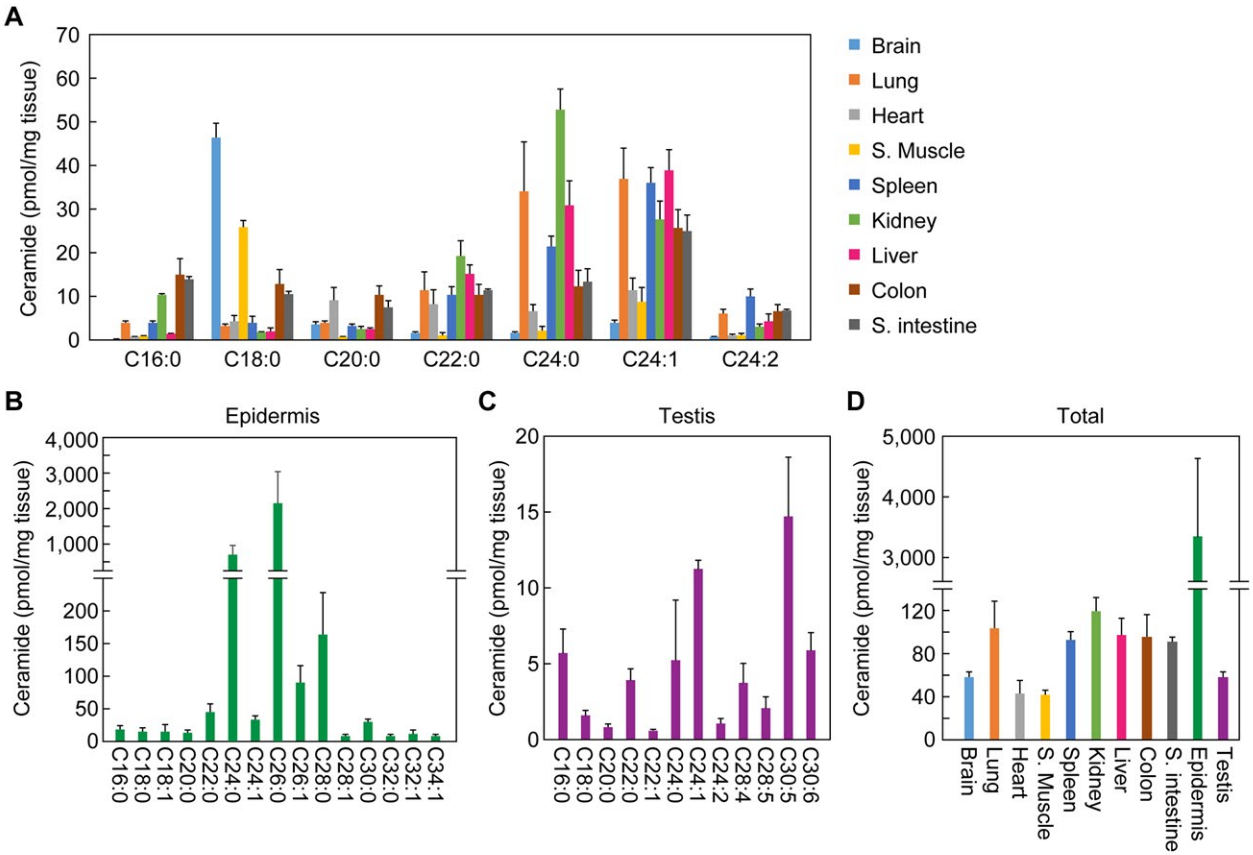
A
Ceramide (pmol/mg tissue)
70
60
50
40
30
20
10
0
C16:0
C18:0
C20:0
C22:0
C24:0
C24:1
C24:2
Brain
Lung
Heart
S. Muscle
Spleen
Kidney
Liver
Colon
S. intestine
B
Epidermis
Ceramide (pmol/mg tissue)
4,000
3,000
2,000
1,000
200
150
100
50
0
C16:0
C18:0
C18:1
C20:0
C22:0
C24:0
C24:1
C26:0
C26:1
C28:0
C28:1
C30:0
C32:0
C32:1
C34:1
C
Testis
Ceramide (pmol/mg tissue)
20
15
10
5
0
C16:0
C18:0
C20:0
C22:0
C22:1
C24:0
C24:1
C24:2
C28:4
C28:5
C30:5
C30:6
D
Total
Ceramide (pmol/mg tissue)
5,000
4,000
3,000
120
80
40
0
Brain
Lung
Heart
S. Muscle
Spleen
Kidney
Liver
Colon
S. intestine
Epidermis
Testis

Figure 3

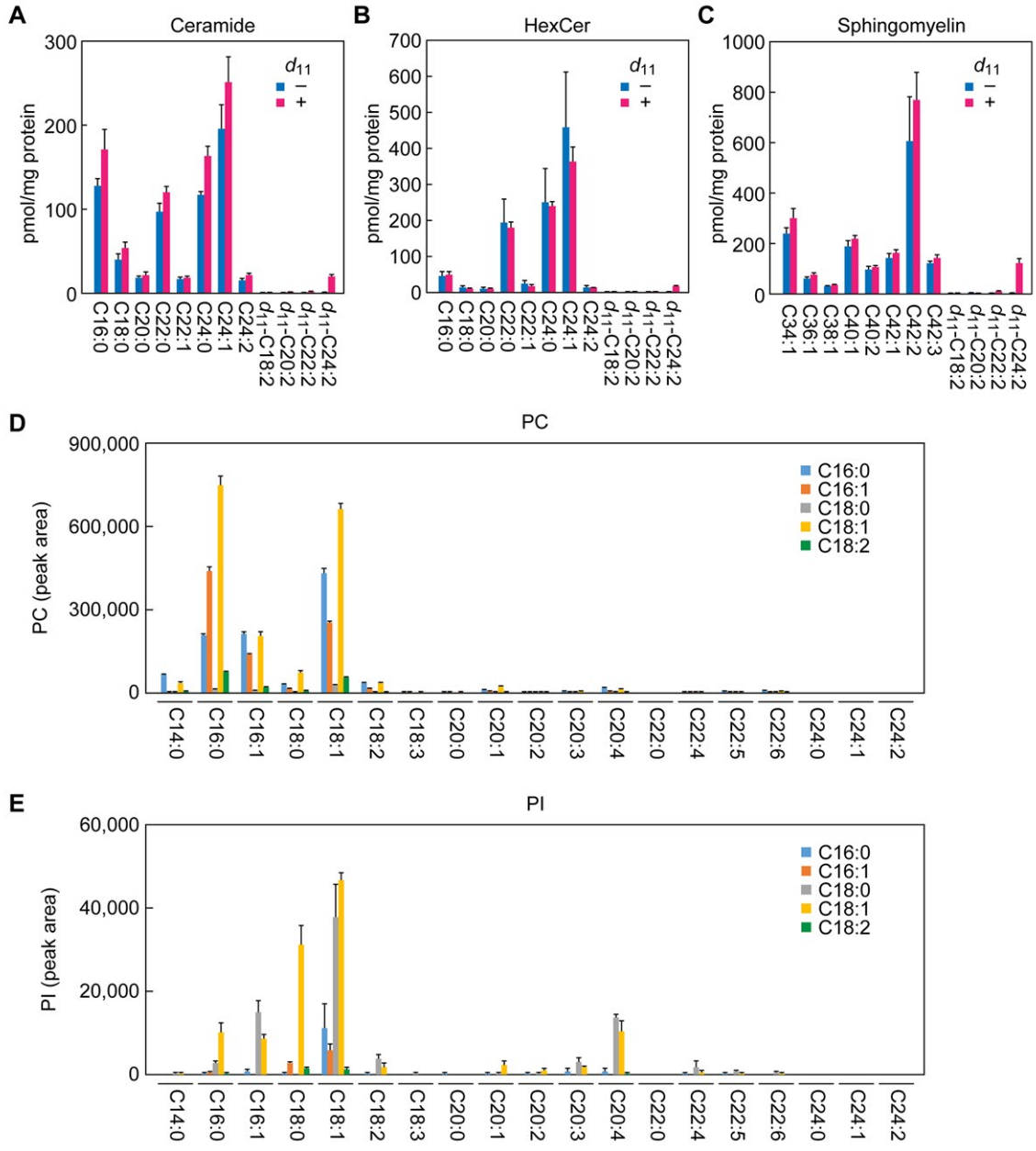
A
Ceramide
pmol/mg protein
300
200
100
0
d_{11}
−
+
C16:0
C18:0
C20:0
C22:0
C22:1
C24:0
C24:1
C24:2
d_{11}-C18:2
d_{11}-C20:2
d_{11}-C22:2
d_{11}-C24:2
B
HexCer
pmol/mg protein
700
600
500
400
300
200
100
0
d_{11}
−
+
C16:0
C18:0
C20:0
C22:0
C22:1
C24:0
C24:1
C24:2
d_{11}-C18:2
d_{11}-C20:2
d_{11}-C22:2
d_{11}-C24:2
C
Sphingomyelin
pmol/mg protein
1000
800
600
400
200
0
d_{11}
−
+
C34:1
C36:1
C38:1
C40:1
C40:2
C42:1
C42:2
C42:3
d_{11}-C18:2
d_{11}-C20:2
d_{11}-C22:2
d_{11}-C24:2
D
PC
PC (peak area)
900,000
600,000
300,000
0
C16:0
C16:1
C18:0
C18:1
C18:2
C14:0
C16:0
C16:1
C18:0
C18:1
C18:2
C18:3
C20:0
C20:1
C20:2
C20:3
C20:4
C22:0
C22:4
C22:5
C22:6
C24:0
C24:1
C24:2
E
PI
PI (peak area)
60,000
40,000
20,000
0
C16:0
C16:1
C18:0
C18:1
C18:2
C14:0
C16:0
C16:1
C18:0
C18:1
C18:2
C18:3
C20:0
C20:1
C20:2
C20:3
C20:4
C22:0
C22:4
C22:5
C22:6
C24:0
C24:1
C24:2

Figure 4

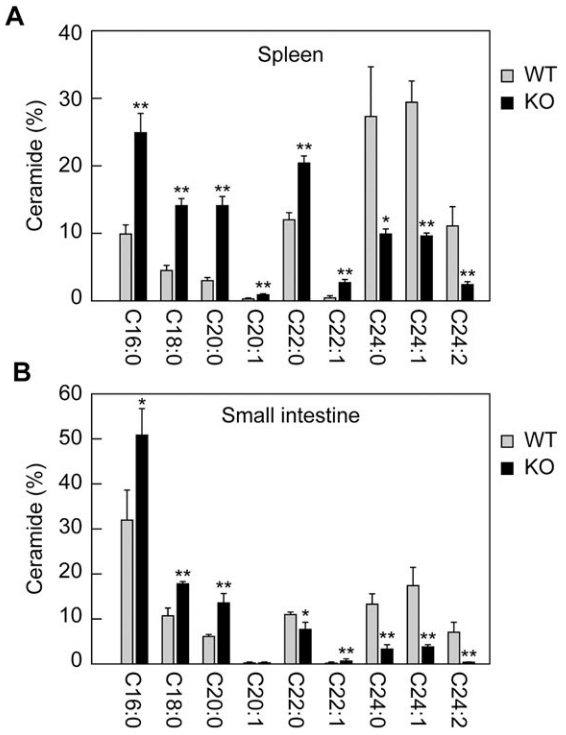
A
Spleen
Ceramide (%)
WT
KO
C16:0
C18:0
C20:0
C20:1
C22:0
C22:1
C24:0
C24:1
C24:2
B
Small intestine
Ceramide (%)
WT
KO
C16:0
C18:0
C20:0
C20:1
C22:0
C22:1
C24:0
C24:1
C24:2

Figure 5

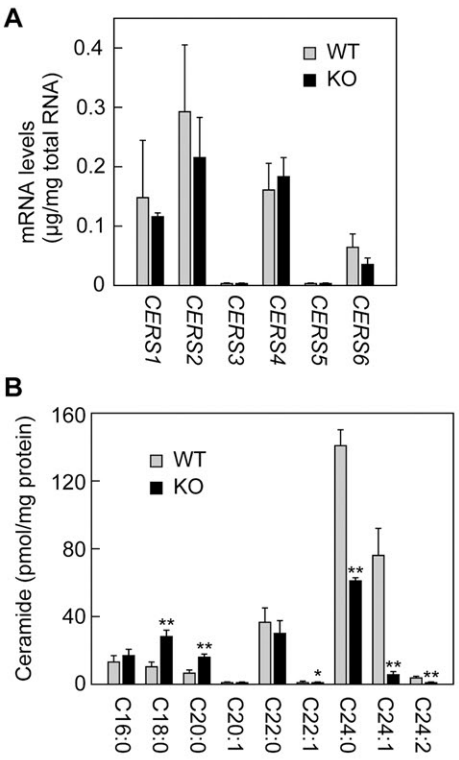
A
mRNA levels (µg/mg total RNA)
0.4
0.3
0.2
0.1
0
WT
KO
CERS1
CERS2
CERS3
CERS4
CERS5
CERS6
B
Ceramide (pmol/mg protein)
160
120
80
40
0
WT
KO
**
**
**
*
**
**
C16:0
C18:0
C20:0
C20:1
C22:0
C22:1
C24:0
C24:1
C24:2

Figure 6

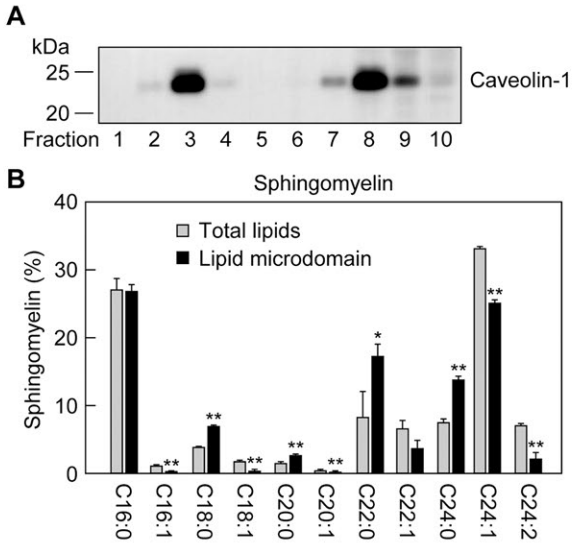
A
kDa
25
20
Caveolin-1
Fraction 1 2 3 4 5 6 7 8 9 10
B
Sphingomyelin
Total lipids
Lipid microdomain
Sphingomyelin (%)
40
30
20
10
0
C16:0
C16:1
C18:0
C18:1
C20:0
C20:1
C22:0
C22:1
C24:0
C24:1
C24:2

Figure 7

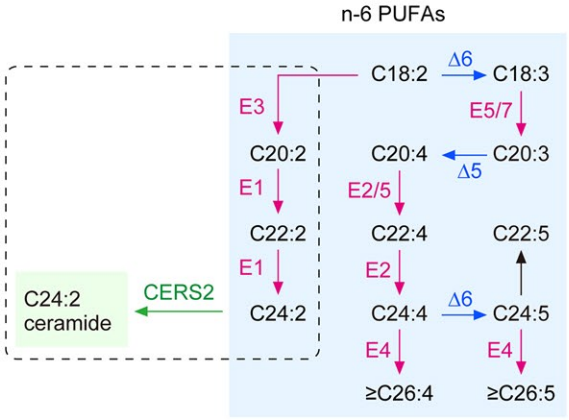
n-6 PUFAs
C18:2
Δ6
C18:3
E3
E5/7
C20:2
C20:4
Δ5
C20:3
E1
E2/5
C22:2
C22:4
C22:5
E1
E2
C24:2
ceramide
CERS2
C24:2
C24:4
Δ6
C24:5
E4
E4
≥C26:4
≥C26:5

Fig. S1

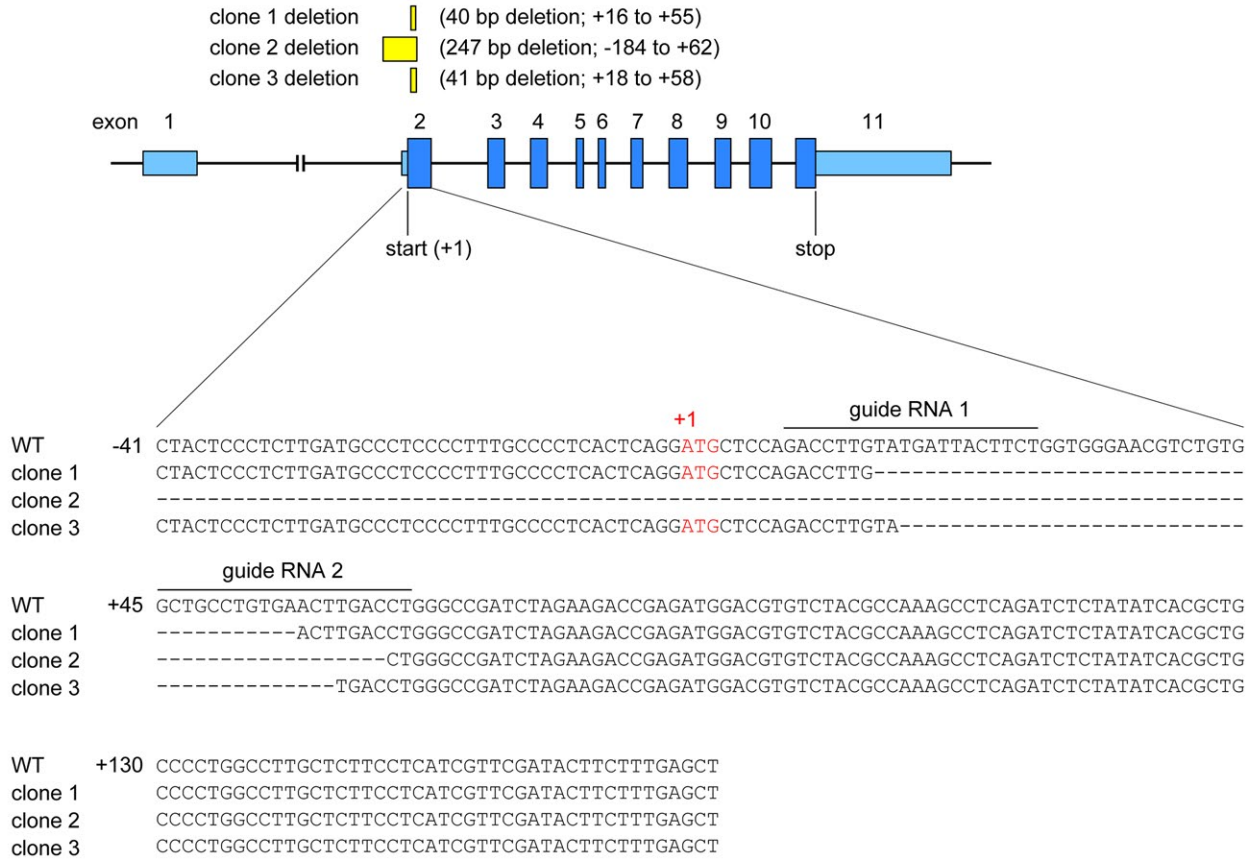
clone 1 deletion (40 bp deletion; +16 to +55)
clone 2 deletion (247 bp deletion; -184 to +62)
clone 3 deletion (41 bp deletion; +18 to +58)
exon 1 2 3 4 5 6 7 8 9 10 11
start (+1)
stop
+1
guide RNA 1
WT -41 CTACTCCCTCTTGATGCCCTCCCCTTTGCCCCTCACTCAGGATGCTCCAGACCTTGTATGATTACTTCTGGTGGGAACGTCTGTG
clone 1 CTACTCCCTCTTGATGCCCTCCCCTTTGCCCCTCACTCAGGATGCTCCAGACCTTG----------
clone 2 ----------
clone 3 CTACTCCCTCTTGATGCCCTCCCCTTTGCCCCTCACTCAGGATGCTCCAGACCTTGTA----------
guide RNA 2
WT +45 GCTGCCTGTGAACTTGACCTGGGCCGATCTAGAAGACCGAGATGGACGTGTCTACGCCAAAGCCTCAGATCTCTATATCACGCTG
clone 1 ----------ACTTGACCTGGGCCGATCTAGAAGACCGAGATGGACGTGTCTACGCCAAAGCCTCAGATCTCTATATCACGCTG
clone 2 ----------CTGGGCCGATCTAGAAGACCGAGATGGACGTGTCTACGCCAAAGCCTCAGATCTCTATATCACGCTG
clone 3 ----------TGACCTGGGCCGATCTAGAAGACCGAGATGGACGTGTCTACGCCAAAGCCTCAGATCTCTATATCACGCTG
WT +130 CCCCTGGCCTTGCTCTTCCTCATCGTTCGATACTTCTTTGAGCT
clone 1 CCCCTGGCCTTGCTCTTCCTCATCGTTCGATACTTCTTTGAGCT
clone 2 CCCCTGGCCTTGCTCTTCCTCATCGTTCGATACTTCTTTGAGCT
clone 3 CCCCTGGCCTTGCTCTTCCTCATCGTTCGATACTTCTTTGAGCT